Radiative forcing due to carbon dioxide decomposed into its component vibrational bands

Received: 15 December 2022 | Revised: 7 March 2023 | Accepted: 10 May 2023

DOI: 10.1002/qj.4485

Quarterly Journal of the Royal Meteorological Society RMetS

RESEARCH ARTICLE

Radiative forcing due to carbon dioxide decomposed into its component vibrational bands†

Keith P. Shine | **Georgina E. Perry**

Department of Meteorology, University of Reading, Reading, UK

Correspondence
Keith P. Shine, Department of Meteorology, University of Reading, Earley Gate, Reading, RG6 6ET, UK.
Email: k.p.shine@reading.ac.uk

Abstract

The radiative forcing (RF) of climate change due to increases in carbon dioxide (CO_2) concentration is primarily in the wavenumber region 500–850 cm^{-1} (wavelengths of approximately 12 to 20 μm). It originates from absorption and emission of infrared radiation due to vibrational–rotational transitions of the CO_2 molecule. While this RF has been the subject of intense and detailed study, to date, the contribution of different vibrational transitions to this forcing has not been explored. This article presents an analysis of radiative transfer calculations that quantify the role of different vibrational transitions and illustrates that while the fundamental bending mode contributes nearly 90% of the total infrared intensity, it contributes less than half of the RF at present-day CO_2 concentrations; this is because the absorption at the centre of this fundamental band is so intense that the effect of additional CO_2 is strongly muted. By successively adding in additional CO_2 bands to the calculations, it is demonstrated that a key spectroscopic phenomenon, known as Fermi Resonance (an interaction between excited states of the bending and the symmetric stretching modes of CO_2) leads to a significant spreading of the infrared intensity to both higher and lower wavenumbers, where the fundamental bending mode is less important. The Fermi Resonance transitions contribute only about 4% of the total infrared intensity in this spectral region but cause more than half of the present-day RF. The less-abundant isotopologues of CO_2 have little impact on the spectrally integrated RF, but this small contribution results from a compensation between more significant positive and negative contributions to the spectral RF. This work does not alter the results of detailed RF calculations available in the literature; rather, it helps explain the physical basis of that forcing.

KEYWORDS

carbon dioxide, Fermi resonance, radiative forcing

†This article is based on Shine's Mason Gold Medal Lecture, delivered at the Royal Meteorological Society Annual General Meeting (8 June 2022).

1 | INTRODUCTION

Changes in CO_2 are the main driver of contemporary climate change. The Sixth Assessment Report of the Intergovernmental Panel on Climate Change (IPCC) (Forster *et al.*, 2021) reports that the changes in CO_2 concentration between 1750 and 2019 resulted in an effective radiative forcing[1] (ERF) of $2.16 \pm 0.24\,W{\cdot}m^{-2}$. This is about 65% of the total well-mixed greenhouse gas forcing and almost 80% of the total anthropogenic ERF ($2.72 \pm 0.76\,W{\cdot}m^{-2}$). (Uncertainties represent the assessed 5–95% uncertainty range).

Many studies have examined the details of the CO_2 RF (e.g. Shine *et al.*, 1995; Zhong and Haigh, 2013; Mlynczak *et al.*, 2016; Dufresne *et al.*, 2020) and shown that most (more than 90%) originates in the wavenumber region 500–850 cm^{-1} (wavelengths 12 to 20 μm). These studies (and as also indicated earlier by Plass (1956), and in the context of possible detection of CO_2 changes in satellite radiances, by Kiehl (1983) and Charlock (1984)) have repeatedly shown that the RF peak does not occur at 670 cm^{-1} (15 μm), where the CO_2 infrared intensity[2] in this spectral region is at its strongest; rather, the maximum forcing occurs at approximately $\pm 60\,cm^{-1}$ either side of this peak, where the intensity is about a factor of 100 weaker. This is explained by the fact that at the wavenumbers around the peak intensity, absorption is already so strong that the effect of the additional CO_2 is strongly muted.

The absorption by CO_2 across the wavenumber region 500–850 cm^{-1} originates from transitions between different vibrational modes of the CO_2 molecule but, to our knowledge, the contribution of these different transitions to CO_2 RF has never been explicitly quantified. This article presents such a quantification. The presentation is partly tutorial in nature as it requires a discussion of some fundamentals of molecular spectroscopy of CO_2 that are rarely discussed in any detail in atmospheric science textbooks. The outcomes of this work do not alter the results of detailed calculations of CO_2 RF; rather, they add to the understanding of fundamental physical mechanisms causing that forcing.

[1]ERF is IPCC's preferred measure of radiative forcing, but it is not amenable to detailed study of the spectral nature of RF; a more restrictive definition is used here, in common with other detailed studies of the spectral nature of CO_2 forcing. This is the instantaneous RF at the tropopause, referred to here as RF, which is the change in the net irradiance at the tropopause following the change in CO_2 concentration, in the absence of any other change; it approximates the spectrally integrated ERF to within a few per cent, as the ERF is estimated to be about 5% higher than the stratospheric-temperature-adjusted RF (SARF: Forster *et al.*, 2021) while the tropopause instantaneous RF is itself calculated to be about 6% higher than SARF (e.g. Shine *et al.*, 1995).

[2]Throughout this article, "intensity" is a measure of the relative probability of absorption or emission of radiation by a CO_2 molecule, in contrast to the occasional (and now dated) usage of intensity as a measure of radiant flux or radiant flux density.

2 | SOME ELEMENTARY MOLECULAR SPECTROSCOPY OF CARBON DIOXIDE

This section summarises several relevant concepts in molecular spectroscopy for readers with less familiarity. More details can be found in some atmospheric texts (e.g. Goody and Yung, 1989) and many molecular spectroscopy texts (e.g. Herzberg, 1945; Banwell and McCash, 1994; Atkins and de Paula, 2010; Bernath, 2016). The focus here will be on CO_2 in the 500–850 cm^{-1} wavenumber region, in which the majority of the CO_2 RF originates.

CO_2 is a symmetric linear triatomic molecule. Infrared absorption by CO_2 results from transitions between different vibrational states of the molecule; these have been well understood since at least the 1930s (e.g. Martin and Barker, 1932). Linear triatomic molecules possess four fundamental modes of vibration (Figure 1). These are conventionally labelled ν_1, which is a symmetric stretch of the two CO bonds, ν_2, which is a bending mode and ν_3, an asymmetric stretch. The ν_2 bending mode accounts for two of the fundamental modes, as the bends that are at right angles to each other constitute independent but otherwise identical modes of vibration (in spectroscopic terminology, the two modes are said to be "degenerate"). The frequencies (and energies) of these vibrational modes are generally reported in wavenumber units (cm^{-1}) and are, respectively, 1330, 667 and 2350 cm^{-1}. The ν_2 mode occurs close to the peak of the Planck Function at typical atmospheric temperatures; hence it is often stated to be the prime source of the CO_2 RF, but as will be shown here,

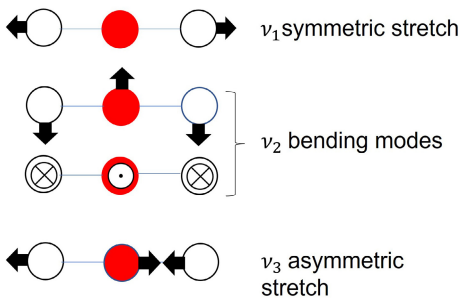

FIGURE 1 Schematic of the different fundamental vibrational modes of CO_2. The ν_2 bending mode has two independent components represented by bending in the plane of the page and bending in and out of the page. [Colour figure can be viewed at wileyonlinelibrary.com]

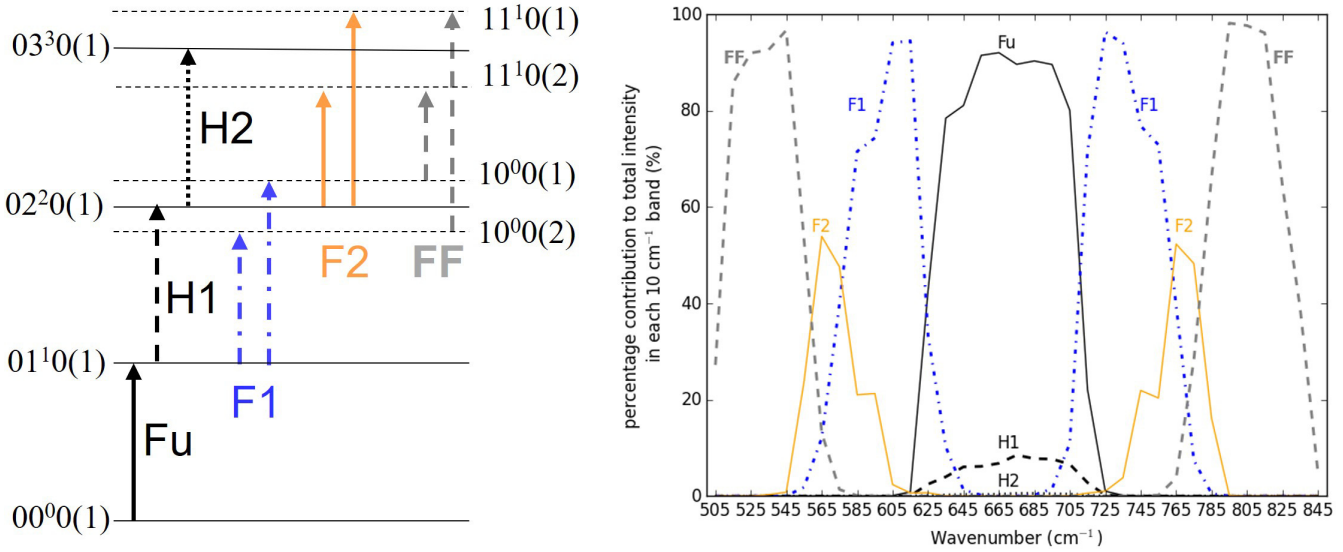

FIGURE 2 Left: energy level schematic showing the principal transitions contributing to CO_2 radiative forcing in the 500–850 cm^{-1} spectral region. Energy levels associated with Fermi pairs are indicated as horizontal dashed lines. Fu, H1 and H2 are the fundamental, first hot band and second hot band transitions, respectively. F1, F2 and FF are the first-Fermi, second-Fermi and Fermi-Fermi transitions, respectively, referred to in the text. The $00^00(1)$ for example nomenclature is explained in Section 3.1 and shown in Table 1. Right: percentage contribution of these different CO_2 vibrational transitions, labelled as in the left of the figure, to the total intensity in each 10 cm^{-1} interval. The figure only includes transitions of the $^{12}C^{16}O_2$ isotopologue. [Colour figure can be viewed at wileyonlinelibrary.com]

such a view is too simplistic. The fact that the wavenumber of the ν_1 symmetric stretch is about double that of the ν_2 bending mode will be shown to be of particular significance.

Infrared absorption and emission occur because of transitions between vibrational states. The states, and the transitions between them, are shown in Figure 2 (left) using a notation that will be explained in detail in Section 3.1. An important determinant of the intensity of a transition from, say, a lower energy state to a higher energy state, is the fraction of the population of molecules (in this case CO_2 molecules) that are in that lower energy state. In the troposphere and stratosphere this fraction is mostly determined by collisions between CO_2 molecules and all other molecules; it primarily depends on temperature, but also on degeneracy, and is described by the Boltzmann distribution. At atmospheric temperatures, lower energy vibrational states are far more populated than higher energy wavenumber states.

In the ground state, the molecule possesses no vibrational quanta (although it still possesses a ground-state energy). When a photon with energy equivalent to 667 cm^{-1} is incident, it can excite the molecule from the ground state to the first excited state of the ν_2 bending mode, leading to absorption in the vicinity of that wavenumber. This is known as the fundamental band (labelled Fu in Figure 2); at atmospheric temperatures it is normally the most intense feature in the 500–850 cm^{-1} spectral region, as more than 90% of CO_2 molecules are in this ground vibrational state. If a molecule is already in the first excited ν_2 state, it can be excited into the second excited ν_2 state, or from the second to the third, and so on. These are called "hot bands" as they become more important when temperature increases in accordance with the Boltzmann distribution because these excited states become more populated. In normal atmospheric conditions, because the fraction of the population of CO_2 molecules decreases markedly between each excited state, each successive hot band is typically a factor of 10 less intense than its predecessor. In shorthand, if v is an integer representing the vibrational level, then the fundamental band is for the transition from $v=0$ to $v=1$, and hot bands are transitions from $v=n$ to $v=n+1$ for $n>0$.

The incident photon does not have to be exactly at a wavenumber of 667 cm^{-1} to cause absorption, for two reasons. The first is that when a molecule changes vibrational state, it can also change rotational state. Rotational levels are separated by much smaller energies than vibrational levels; these add important structure to the vibrational transitions. As a result of quantum mechanical selection rules, only certain rotational transitions are allowed when a vibrational transition occurs. A one-quantum increase in the ν_2 bending mode can be accompanied by either a decrease in one quantum of rotational energy, no change in rotational energy or an increase in one quantum of rotational energy. Or, if J is an integer that represents the original rotational level, then the allowed vibrational transitions are those where $\Delta J = \pm 1$ or 0.

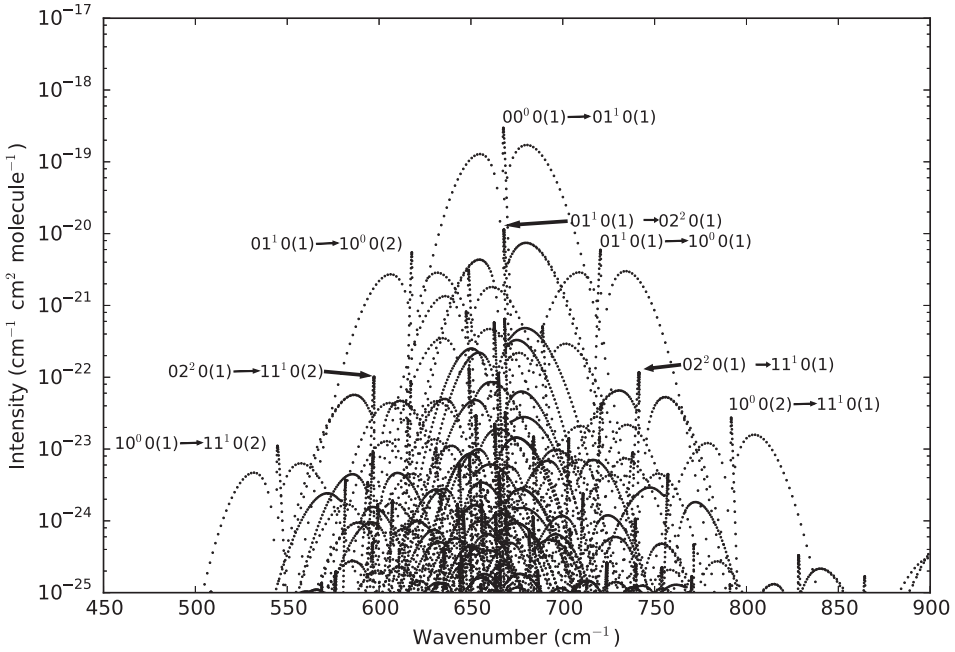

FIGURE 3 Vibrational-rotation lines of CO_2 in the 500–850 cm^{-1} spectral region. Each dot represents the line intensity (in cm^{-1} cm^2 molecule^{-1}) at the centre of an individual vibration–rotation transition. The Q branch of transitions of particular importance in determining the RF are labelled. Data taken from HITRAN2020 (Gordon *et al.*, 2022).

Unlike the vibrational energy levels, which are almost equally spaced in energy, rotational energy levels are not; they become more widely spaced as rotational energy increases. A consequence of this is that the wavenumber of a one-quantum change in rotational energy following a vibrational transition depends on the number of quanta of rotational energy that the molecule possesses in the initial vibrational state. This leads to a characteristic structure in vibrational-rotation spectra which is illustrated in Figure 3, which shows the intensity of absorption lines at their line centre for individual vibration–rotation features. Focusing, for now, on the most intense absorption band (the ν_2 fundamental band) the sharp feature at around 667 cm^{-1} is known as the Q branch, where the vibrational transition is accompanied by no change in rotational energy. The set of transitions at lower wavenumbers are known as the P branch, which are associated with a one-quantum decrease in rotational energy. The set of transitions at higher wavenumbers are the R branch, associated with a one-quantum increase in rotational energy. Transitions in the P and R branch (which are associated with different initial rotational energies) are typically separated by a few cm^{-1}. The Q branch has its own sub-structure but with a much smaller spacing (typically 0.1 cm^{-1}) of absorption lines. For cases considered here, the Q branch (no change in rotational level) is allowed; it is not allowed for transitions involving the ν_3 asymmetric stretch.

The second reason that the incident photon does not have to be exactly at a wavenumber of 667 cm^{-1} is that each individual vibrational-rotation absorption line is broadened around its centre. In the troposphere this is mostly due to molecular collisions; at 1000 hPa this broadening leads to a half-width of 0.05 to 0.1 cm^{-1} and decreases approximately linearly with decreasing pressure. This leads to some overlap of absorption lines, especially the narrowly spaced Q branch transitions.

A key selection rule determining the intensity, or even the existence, of a transition in a molecule's atmospheric spectrum, is whether the stretch or bending vibrations cause a time-varying change in the electric dipole associated with the molecule. It is this change in electric dipole that allows interaction with the radiation field, leading to either absorption or emission of a photon. Because of its symmetry, in its "resting" state (Figure 1), the CO_2 molecule does not possess an electric dipole. It is equally positively charged at both ends. It remains that way for the ν_1 symmetric stretch and so, on its own, this mode is not infrared active; hence it is often ignored in atmospheric texts. By contrast, both the ν_2 bending mode and ν_3 asymmetric stretch do lead to a time-varying electric dipole and so are infrared active. Although the ν_3 band is spectroscopically more intense than ν_2, it is centred at 2350 cm^{-1} (about 4.3 μm) where both incoming (from the Sun) and outgoing (from the Earth and atmosphere) irradiances are relatively low; therefore, it is of much less importance from the perspective of the Earth's energy balance and RF.

A key concept for this article is that as well as transitions involving a single vibrational mode, transitions (called combination bands) occur which involve changes in two (or more) vibrational modes. A particularly important example here is the transition from the first excited state of the ν_2 bending mode (at around 667 cm^{-1}) to the

first excited state of the ν_1 symmetric stretch (at about 1,330 cm^{-1}). These two states are separated by ≈663 cm^{-1} and hence this transition falls in the wavenumber region of interest here.

As noted earlier, the energy of the first excited ν_1 state is almost identical to the second excited state of ν_2. This leads to an interaction between these two states known as Fermi Resonance (e.g. Herzberg, 1945; Goody and Yung, 1989; Bernath, 2016). In quantum mechanical terms, the wave functions of these two states mix, leading to two distinct states; a classical interpretation (e.g. Herzberg, 1945) is that the bend and symmetric stretch interact as coupled oscillators. What is most important here is the *consequence* of Fermi Resonance. Instead of two states (ν_1 and 2 ν_2) existing at about 1,330 cm^{-1}, there are two distinct Fermi states centred at about ±50 cm^{-1} either side of 1,330 cm^{-1} (an elaboration on this will be explained in Section 4); these are illustrated by the lower pair of horizontal dashed lines in Figure 2 (left). This means that transitions from the first excited ν_2 state to these two distinct states (labelled F1 in Figure 2 [left]) are themselves shifted away from the wavenumber of the fundamental ν_2 band; this will be shown to have a marked impact on the CO_2 spectrum and the associated RF. Other excited modes of vibration of CO_2 show Fermi Resonance, and transitions to and from these Fermi states (Figure 2 [left]) add richness to the CO_2 spectrum, as will be shown in Section 4. It is because of Fermi Resonance that the apparently infrared-inactive ν_1 symmetric stretch becomes important from an atmospheric perspective.

A final consideration here is that 98.4% of CO_2 in the atmosphere is the main isotopologue $^{12}C^{16}O_2$ (Gordon *et al.*, 2022), but many other CO_2 isotopologues are present. The three most abundant (abundances are from Gordon *et al.* (2022)) are $^{13}C^{16}O_2$ (about 1.1%), $^{16}O^{12}C^{18}O$ (about 0.4%) and $^{16}O^{12}C^{17}O$ (about 0.07%). Other isotopologues are more than an order of magnitude less abundant than $^{16}O^{12}C^{17}O$. These isotopologues have slightly different spectral characteristics to $^{12}C^{16}O_2$ because of the change in mass and, in the case of $^{16}O^{12}C^{18}O$ and $^{16}O^{12}C^{17}O$, because of the removal of the symmetry of the molecule (see Section 5).

Mlynczak *et al.* (2016) discuss other spectroscopic processes to assess their importance for CO_2 RF. One of these, known as line mixing, occurs when molecular collisions mean that nearby vibration–rotation lines cannot be considered isolated from each other; this results in a transfer of intensity between them. Mlynczak *et al.* (2016) show that line mixing has a negligible (around 0.2%) impact on the calculated CO_2 RF across the 500–2,200 cm^{-1} spectral region, because of strongly compensating negative and positive changes in the spectrally resolved RF, that result from slight shifts (of the order of the line half-width) in that spectrum. Because of this small impact on the forcing, line mixing is not considered further here.

3 | METHODOLOGY

3.1 | The HITRAN spectroscopic database and notation

Individual vibration–rotation lines of most gases of atmospheric interest are catalogued on the regularly updated High-resolution Transmission molecular absorption (HITRAN) spectroscopic database (Gordon *et al.*, 2022). For each spectral line, HITRAN lists many parameters, as well as uncertainty estimates. For present purposes, the three most important parameters are the wavenumber of line centre (in cm^{-1}), its intensity at 296 K (which is a measure of the probability of a particular transition occurring), reported in the standard spectroscopic units of $cm^{-1}\cdot(molecule\cdot cm^{-2})^{-1}$, and the collision-broadened line half-width at standard temperature and pressure (in cm^{-1}). For CO_2, HITRAN catalogues over 100,000 individual spectral lines, across 12 isotopologues, in the 500–850 cm^{-1} spectral interval, with over 200 different vibrational transitions for the main isotopologue alone.

HITRAN uses a notation to indicate the vibrational states involved in each transition (and an accompanying notation for the change in rotational state, which will not be used here). For CO_2 each state is denoted by $\nu_1\ \nu_2{}^l\ \nu_3(n)$ where $\nu_1\ \nu_2\ \nu_3$ indicates the number of quanta of each vibrational mode. The superscript l on ν_2 arises because of the two components of that mode mentioned in Section 2. If both modes are active at the same time, then, depending on their phase, there can be a (quantized) rotation (and hence rotational energy) associated with the vibration. The presence of this rotational energy influences the occurrence of Fermi Resonance as will be noted later. The (n) notation is used in indicating Fermi Resonance, as will also be explained shortly.

The ground state of CO_2 is $00^00(1)$ but we are interested here in transitions between states. The fundamental ν_2 band is given by $00^00(1) \rightarrow 01^10(1)$ (all examples given here assume absorption rather than emission of a photon, but both are important for RF), and the hot bands are given by $01^10(1) \rightarrow 02^20(1)$, $02^20(1) \rightarrow 03^30(1)$ for example.

A transition labelled $01^10(1) \rightarrow 02^00(1)$ might seem possible, but the 02^00 and 10^00 states are Fermi resonant and form two distinct states that are, instead, by convention, labelled $10^00(1)$ and $10^00(2)$. Hence, the two transitions from $01^10(1)$ to these Fermi states are labelled $01^10(1) \rightarrow 10^00(1)$ and $01^10(1) \rightarrow 10^00(2)$. The higher Fermi index state ($10^00(2)$) is centred at an energy of about 100 cm^{-1} lower than the $10^00(1)$ state and hence

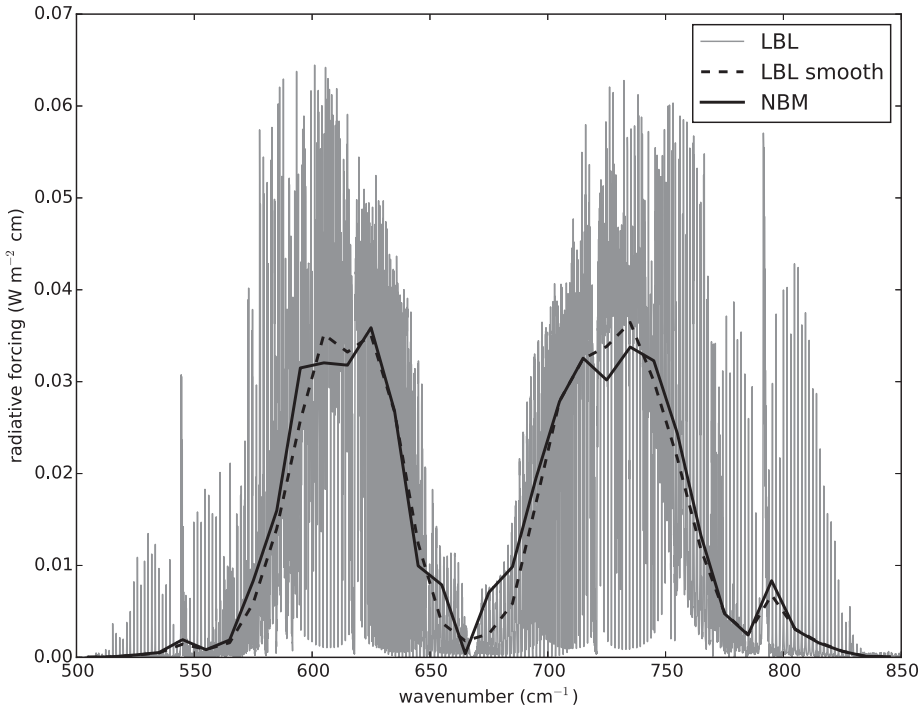

FIGURE 4 Instantaneous radiative forcing at the tropopause for an increase in CO_2 mole fraction from 410 to 820 ppm. The grey line shows the line-by-line calculations, the solid black line the narrow-band calculations and the dashed black line the line-by-line (LBL) calculations smoothed to the 10 cm^{-1} spectral resolution of the narrow-band model (NBM).

the two transitions from $01^10(1)$ are separated by about 100 cm^{-1}. Fermi Resonance is not associated with the nearby (in energy terms) 02^20 state, as it only occurs when the wave functions of the two interacting states share the same symmetry characteristics. Sometimes more than two Fermi states can occur (for example, $20^00(1)$, $20^00(2)$, $20^00(3)$) and several different Fermi states can exist around a given ν_2 excited state.

Although some combination band transitions involving the ν_3 asymmetric stretch can occur in the 500–850 cm^{-1} region, none are intense enough to be considered separately here. The ν_3 mode does play a role in two CO_2 bands near 950 and 1,050 cm^{-1} (i.e. near wavelengths of 10 μm), associated with transitions from the Fermi pair $10^00(1)$ and $10^00(2)$ to $00^01(1)$. These contribute around 5% to the total CO_2 thermal infrared RF (e.g. Augustsson and Ramanathan, 1977; Mlynczak *et al.*, 2016) for CO_2 doubling from pre-industrial concentrations; Augustsson and Ramanathan (1977) and Zhong and Haigh (2013) demonstrate that these bands becomes progressively more important as CO_2 concentrations increase.

For the calculations presented here, the list of lines associated with individual vibrational transitions had to be extracted from HITRAN to enable the calculation of the contribution of these transitions.

3.2 | Radiative transfer code

To calculate the RF associated with each vibrational transition, the 10 cm^{-1} spectral-resolution narrow-band radiative transfer code described in Shine and Myhre (2020) is used. Unlike some radiative transfer codes, this directly uses HITRAN data as input, and hence it was more straightforward to perform the necessary calculations involving a subset of CO_2 vibrational transitions. HITRAN2020 (Gordon *et al.*, 2022) is used, together with Version 3.2 of the MT-CKD water vapour continuum (Mlawer *et al.*, 2019). Since the calculations presented here are primarily to illustrate processes, a single global-mean profile of temperature, water vapour and ozone is used, with clouds specified at three levels (Freckleton *et al.*, 1998). Calculations include CO_2, N_2O and CH_4 at present-day mole fractions (410 ppm, 323 ppb and 1800 ppb respectively) and are assumed to be well-mixed. For gases other than CO_2, all spectral lines catalogued on HITRAN are included in the calculations. As noted, attention is focused on the 500–850 cm^{-1} spectral region. The variations of line intensity with temperature and line width with temperature and pressure are included in the radiative transfer calculations.

Instantaneous RF calculations are performed for a change in CO_2 mole fraction from 410 to 820 ppm, with the focus on the tropopause forcing. Figure 4 compares the narrow-band forcing against the line-by-line code of Dudhia (2017) when all CO_2 vibrational bands are included, for cloudless conditions. The line-by-line forcing compares well with similar calculations of Mlynczak *et al.* (2016). Figure 4 shows that the narrow-band model performs adequately for present purposes. The wavenumber-integrated forcing is 4.58 W·m^{-2} in the

TABLE 1 Role of different vibrational bands to the total infrared intensity and radiative forcing (RF).

Bands included	Lower state	Upper state	Approx. band centre (cm^{-1})	Cumulative contribution to 500–850 cm^{-1} intensity (%)	Cumulative wavenumber integrated forcing ($W \cdot m^{-2}$)	Cumulative contribution to 550–850 cm^{-1} forcing (%)
Fundamental ν_2	$00^00(1)$	$01^10(1)$	670	87.5	1.98	47
Plus hot ν_2	$01^10(1)$	$02^20(1)$	670	94.7	1.89	45
	$02^20(1)$	$03^30(1)$	670			
Plus first Fermi	$01^10(1)$	$10^00(1)$	720	98.0	3.59	86
	$01^10(1)$	$10^00(2)$	620			
Plus second Fermi	$02^20(1)$	$11^10(1)$	740	98.4	3.95	95
	$02^20(1)$	$11^10(2)$	600			
Plus Fermi-Fermi	$10^00(1)$	$11^10(2)$	550	98.5	4.11	99
	$10^00(2)$	$11^10(1)$	795			
All $^{12}C^{16}O_2$				98.6	4.18	100
All (500–850 cm^{-1})				100	4.17	100
All (0–3,000 cm^{-1})					4.47	

Note: Lower and upper state descriptors for the added bands (columns 2 and 3); approximate band centres for each added band (cm^{-1}) (column 4); cumulative fractional contribution of all added CO_2 vibrational bands to the total intensity (at 296 K) in the 550–850 cm^{-1} spectral region (column 5); cumulative wavenumber-integrated RF ($W \cdot m^{-2}$) due to the addition of these bands for a CO_2 mole fraction change from 410 to 820 ppm (column 6); cumulative fractional contribution of all added bands to the total 500–850 cm^{-1} RF (column 7). The final row shows the total thermal infrared RF for all CO_2 bands in the 0–3,000 cm^{-1} spectral region. For reference, the total 500–850 cm^{-1} intensity at 296 K is 9.1×10^{-18} cm^{-1} (molec cm^{-2})$^{-1}$.

narrow-band model and 4.37 $W \cdot m^{-2}$ in the line-by-line model, a difference of 4.8%.

The calculation of the contribution of individual vibrational transitions could be done in several different ways. The chosen method here is to start with the fundamental ν_2 band, as it is dominant in terms of infrared intensity, add in the ν_2 hot bands and then add in successive pairs of Fermi transitions, before presenting calculations including all bands of the main CO_2 isotopologue and then including all bands of all CO_2 isotopologues listed on HITRAN2020.

4 | SPECTRAL CONTRIBUTION OF DIFFERENT CO_2 BANDS

The first step is to investigate the contribution of each band to the total CO_2 intensity (including all isotopologues at their atmospheric abundance) in each 10 cm^{-1} interval from 500 to 850 cm^{-1}, at 296 K. This is calculated from the sum of all line intensities ($\sum_i S_i$ where S_i is the line intensity of the ith line) in each interval (accepting that, when broadened, lines at the boundary of each interval may "leak" some intensity into neighbouring intervals) and the sum of intensities of each individual vibrational band in those 10 cm^{-1} intervals. Intensity is not the only determinant of radiative impact, although it will be shown here that it is effective in identifying the bands that contribute most to CO_2's RF. The radiative transfer code (Section 3.2) also uses the sum of the square root of the product of intensity and half-width, $\sum_i (S_i \alpha_i)^{0.5}$, where α_i is the half-width of the ith line, which is appropriate in the strong limit (e.g. Goody and Yung, 1989; Pierrehumbert, 2010); for this limit, absorption near line centres is saturated and most of the transmittance change, when CO_2 concentrations change, occurs in the line wings.

The purpose here was to identify the dominant contributors to intensities in each 10 cm^{-1} band. Figure 2 (right) shows the proportion of the total intensity due to individual $^{12}C^{16}O_2$ bands, associated with the transitions in Figure 2 (left).

Figure 2 (right) shows the contribution of the fundamental ν_2 band and the first two hot bands (as listed in Table 1), labelled Fu, H1 and H2. Between 610 to 730 cm^{-1} the fundamental and first hot band contribute almost all the infrared intensity but contribute little outside this interval. The two Fermi transitions (labelled F1 in Figure 2) from the $01^10(1)$ state (referred to here as the "first Fermi" – see Table 1) play a major role in broadening the wavenumber of CO_2 absorption; their peak contribution exceeds 90% at wavenumbers near 600 and 730 cm^{-1}. The two Fermi transitions (labelled F2 in Figure 2) from the $02^20(1)$ state (referred to here as "second Fermi" – see

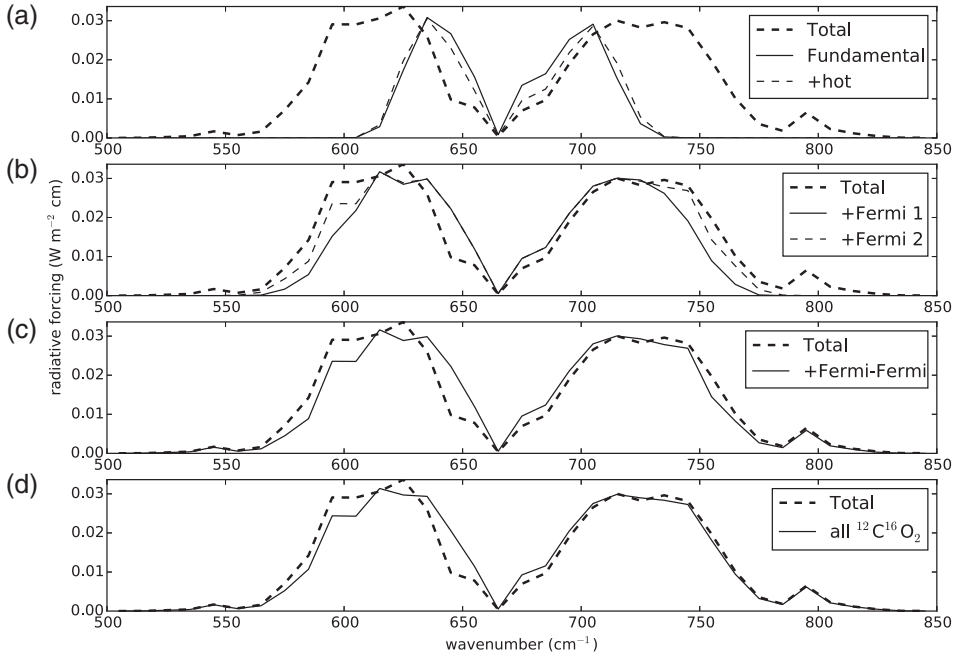

FIGURE 5 Radiative forcing (in W·m^{-2}·(cm^{-1})$^{-1}$) in each 10 cm^{-1} band for an increase in CO_2 mole fraction from 410 to 820 ppm. In each frame the bold dashed line shows the total forcing when all vibrational bands of all CO_2 isotopologues are included. (a) Forcing from the fundamental ν_2 band (solid line) and when ν_2 hot bands (dashed) of $^{12}C^{16}O_2$ are added. (b) Forcing when the first (solid line) and second Fermi (dashed) bands of $^{12}C^{16}O_2$ are added. (c) Forcing when the Fermi-Fermi bands (solid line) of $^{12}C^{16}O_2$ are added. (d) Forcing when all $^{12}C^{16}O_2$ bands (solid line) are added.

Table 1) occur at higher and lower wavenumbers than the first Fermi pair, as the $11^10(1)$ and $11^10(2)$ energy levels are separated from the $03^30(1)$ energy by about ±70 cm^{-1} rather than ±50 cm^{-1} as is the case for F1. Although their peak contributions are only 50%, because of the strong overlap with the first Fermi bands (Figure 3), their role in broadening the range of wavenumbers is also clear. The final transitions shown in Figure 2, and labelled FF, are from the lowest and highest energy of the first Fermi states ($10^00(2)$ and $10^00(1)$) to the highest and lowest energies of the second Fermi states ($11^10(1)$ and $11^10(2)$) (referred to here as "Fermi-Fermi" – see Table 1); although weak in total intensity (Figure 3), these contribute almost all the intensity at the edges of the 500–850 cm^{-1} region. They occur at around ±120 cm^{-1} either side of the fundamental because of the differing separations of the first and second Fermi states.

5 | RADIATIVE FORCING CONTRIBUTION OF DIFFERENT CO_2 BANDS

Figure 5 shows the contribution of each band, as they are added successively, to the spectral RF. In all panels, the bold-dashed line shows the total RF due to all bands and all isotopologues of CO_2. Figure 5a shows the contribution of the fundamental and then the fundamental plus the hot bands. Table 1 shows the wavenumber-integrated forcing. It is immediately apparent that the fundamental band explains only a relatively small proportion of the total forcing (47%) despite contributing around 87% of the total infrared intensity; the contribution of the fundamental plus hot bands to the forcing is smaller (45%). Figure 5a shows that together the fundamental and hot band forcing is restricted to the 600–750 cm^{-1} region; it also shows that at some wavenumbers, the addition of hot bands decreases the forcing (most obviously towards the fundamental band centre) while at others it increases it (e.g. between 700 and 750 cm^{-1}). A simple explanation of this behaviour emerges from considering that the forcing will be related to the rate of change of absorptance with CO_2 concentration, and how this rate of change depends on the optical depth. At low optical depth, this rate of change increases as additional absorbing bands are added; at high optical depth it decreases. This is explained further in the Appendix.

Figure 5b shows the addition of the first Fermi and second Fermi bands. The first set has a particularly dramatic impact on the forcing; while only containing about 3% of the infrared intensity, it almost doubles the wavenumber-integrated RF (Table 1) and, together with the fundamental, explains much of the total spectral variation of CO_2 RF. This is accentuated by the second Fermi bands. However, the relatively small but marked features at around 550 and 800 cm^{-1} are not explained; Figure 5c shows that these are almost entirely explained by the Fermi-Fermi transitions.

Figure 5d shows the total forcing due to $^{12}C^{16}O_2$; the solid line shows only minor deviations from the solid line in Figure 5c which shows that almost all $^{12}C^{16}O_2$ forcing is explained by the bands included in Figure 5a–c.

The difference between the solid and bold-dashed lines in Figure 5d shows the impact of other CO_2 isotopologues.

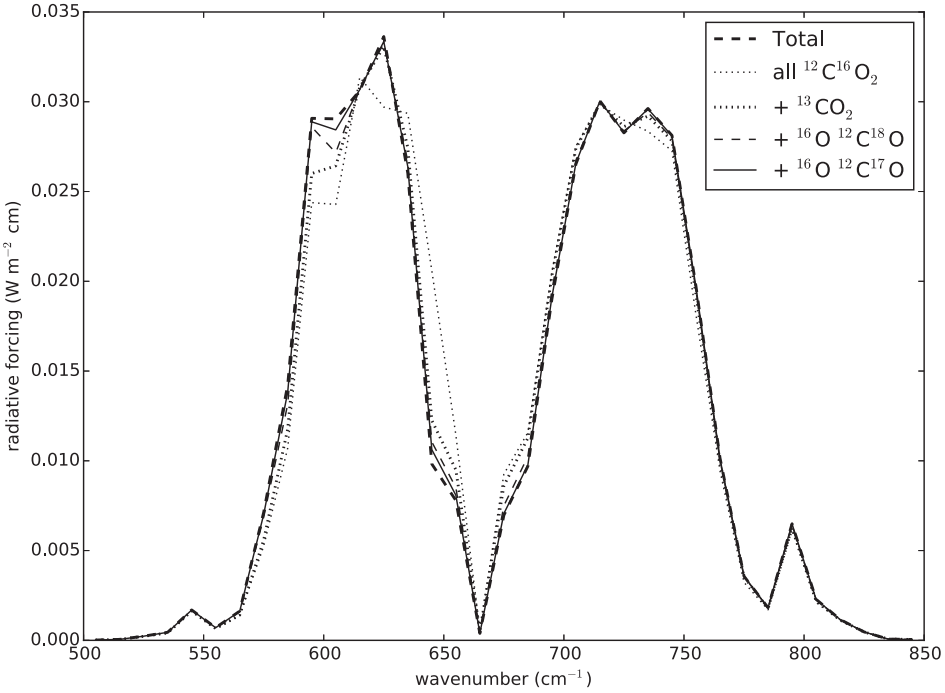

FIGURE 6 Impact of isotopologues on radiative forcing (in $W \cdot m^{-2} \cdot (cm^{-1})^{-1}$) in each 10 cm^{-1} band for an increase in CO_2 mole fraction from 410 to 820 ppm. The figure helps explain the difference between the two curves in Figure 5d by successively adding $^{13}CO_2$, $^{16}O^{12}C^{18}O$ and $^{16}O^{12}C^{17}O$ to $^{12}C^{16}O_2$.

In the wavenumber-integrated sense, they have almost no impact on the total 500–850 cm^{-1} forcing (Table 1). However, Figure 5d shows that the contribution in individual spectral intervals (notably the decreased forcing near 650 cm^{-1} and the increased forcing near 625 and 600 cm^{-1}) is quite marked despite these isotopologues contributing only 1.4% of the total integrated intensity. Much of their role originates from increasing absorption and emission in the wings of $^{12}C^{16}O_2$ lines when the centres of those lines are already saturated over typical atmospheric paths. In this "strong" limit, it is the contribution of the isotopologues to $\sum_i (S_i \alpha_i)^{0.5}$ rather than $\sum_i S_i$ (the "weak" limit) that dictates the change in transmittance as CO_2 increases. The square root means that weaker lines have a greater influence in the strong limit than in the weak limit. In addition, in the case of $^{16}O^{12}C^{17}O$ and $^{16}O^{12}C^{18}O$, the loss of molecular symmetry means that there are more P and R branch lines, which are less intense but more finely spaced than is the case for $^{12}C^{16}O_2$ (e.g. Banwell and McCash, 1994). This also enhances their contribution to $\sum_i (S_i \alpha_i)^{0.5}$.

Figure 6 shows the impact of successively adding $^{13}CO_2$, $^{16}O^{12}C^{18}O$ and $^{16}O^{12}C^{17}O$ to $^{12}C^{16}O_2$ and illustrates that these four isotopologues explain almost all the CO_2 forcing (i.e. the solid line and the bold dashed line are almost coincident). To our knowledge, the RF role due to these isotopologues has not previously been reported. The change in the centre of mass of $^{13}CO_2$ means the Q branch of its fundamental ν_2 band is shifted to 650 cm^{-1}, unlike the other isotopologues considered here, which occur near 667 cm^{-1}. This is the prime cause of the decreased spectral forcing near 650 cm^{-1}. The P branch of this mode explains most of the increased spectral forcing near 625 cm^{-1}. The increased spectral forcing near 600 cm^{-1} is due to the $01^10(1) \rightarrow 10^00(2)$ transition of each of the three rare isotopologues, each of which makes a significant contribution to that increased forcing.

6 | CONCLUSIONS

This article has quantified the contribution of individual vibration–rotation bands to the radiative forcing due to increasing concentrations of CO_2. Although these bands have long been included in radiative transfer calculations, and the wavenumber variation of the CO_2 radiative forcing is well established, to our knowledge the role of these individual bands has not been quantified. Hence this work is meant to be a didactic contribution that aids understanding of the physical origins of the forcing. It could undoubtedly be extended, for example via line-by-line calculations, and to a wider range of atmospheric profiles.

The important role of Fermi Resonance in approximately doubling the radiative forcing due to CO_2 has been highlighted; this is because these resonances broaden the spectral range of CO_2's radiative influence away from wavelength regions where the CO_2 infrared intensity is high and where its forcing is largely saturated at contemporary concentrations. Almost all the spectral radiative forcing is explained by eight vibration–rotation bands of the main CO_2 isotopologue,

plus two vibration–rotation bands of the next three most abundant isotopologues.

AUTHOR CONTRIBUTIONS

Keith P. Shine: Conceptualization; investigation; methodology; supervision; writing – original draft; writing – review and editing. **Georgina E. Perry:** Investigation; methodology; visualization; writing – review and editing.

ACKNOWLEDGEMENTS

Jon Elsey is thanked for his help with the line-by-line calculations and for useful discussions. Comments from Joanna Haigh and an anonymous reviewer helped improve the article.

DATA AVAILABILITY STATEMENT

The spectroscopic data used in these calculations are openly available at https://hitran.org/.

ORCID

Keith P. Shine https://orcid.org/0000-0003-2672-9978

REFERENCES

Atkins, P.W. and De Paula, J. (2010) *Atkins' Physical Chemistry*, 9th edition. Oxford: Oxford University Press.

Augustsson, T. and Ramanathan, V. (1977) A radiative-convective model study of CO_2 climate problem. *Journal of the Atmospheric Sciences*, 34, 448–451. https://doi.org/10.1175/1520-0469(1977)034<0448:arcmso>2.0.co;2.

Banwell, C.N. and McCash, E.M. (1994) *Fundamentals of Molecular Spectroscopy*. London, UK: McGraw-Hill Book Company.

Bernath, P.F. (2016) *Spectra of Atoms and Molecules*, 3rd edition. New York: Oxford University Press.

Charlock, T.P. (1984) CO_2 induced climatic-change and spectral variations in the outgoing terrestrial infrared radiation. *Tellus Series B-Chemical and Physical Meteorology*, 36, 139–148. https://doi.org/10.3402/tellusb.v36i3.14884.

Dudhia, A. (2017) The reference forward model (RFM). *Journal of Quantitative Spectroscopy and Radiative Transfer*, 186, 243–253. https://doi.org/10.1016/j.jqsrt.2016.06.018.

Dufresne, J.-L., Eymet, V., Crevoisier, C. and Grandpeix, J.-Y. (2020) Greenhouse effect: the relative contributions of emission height and total absorption. *Journal of Climate*, 33, 3827–3844. https://doi.org/10.1175/jcli-d-19-0193.1.

Forster, P., Storelvmo, T., Armour, K., Collins, W., Dufresne, J.-L., Frame, D., Lunt, D.J., Mauritsen, T., Palmer, M.D., Watanabe, M., Wild, M. and Zhang, H. (2021) The Earth's energy budget, climate feedbacks, and climate sensitivity. In: Masson-Delmotte, V., et al. (Eds.) *Climate Change 2021: The Physical Science Basis. Contribution of Working Group I to the Sixth Assessment Report of the Intergovernmental Panel on Climate Change*. Cambridge, and New York: Cambridge University Press, pp. 923–1054. https://doi.org/10.1017/9781009157896.009.

Freckleton, R.S., Highwood, E.J., Shine, K.P., Wild, O., Law, K.S. and Sanderson, M.G. (1998) Greenhouse gas radiative forcing: effects of averaging and inhomogeneities in trace gas distribution. *Quarterly Journal of the Royal Meteorological Society*, 124, 2099–2127. https://doi.org/10.1256/smsqj.55013.

Goody, R.M. and Yung, Y.L. (1989) *Atmospheric Radiation: Theoretical Basis*. New York/Oxford: Oxford University Press.

Gordon, I.E. and Coauthors, Karlovets, E.V., Skinner, F.M., Conway, E.K., Hill, C., Kochanov, R.V., Tan, Y. and Wcisło, P. (2022) The HITRAN2020 molecular spectroscopic database. *Journal of Quantitative Spectroscopy & Radiative Transfer*, 277, 107949. https://doi.org/10.1016/j.jqsrt.2021.107949.

Herzberg, G. (1945) *Molecular Spectra and Molecular Structure: II Infrared and Raman Spectra of Polyatomic Molecules*. Princeton, New Jersey: D. Van Nostrand Company, Inc..

Kiehl, J.T. (1983) Satellite detection of effects due to increased atmospheric carbon-dioxide. *Science*, 222, 504–506. https://doi.org/10.1126/science.222.4623.504.

Martin, P.E. and Barker, E.F. (1932) The infrared absorption spectrum of carbon dioxide. *Physical Review*, 41, 219–303. https://doi.org/10.1103/PhysRev.41.291.

Mlawer, E.J. and Coauthors. (2019) Analysis of water vapor absorption in the far-infrared and submillimeter regions using surface radiometric measurements from extremely dry locations. *Journal of Geophysical Research-Atmospheres*, 124, 8134–8160. https://doi.org/10.1029/2018jd029508.

Mlynczak, M.G., Daniels, T.S., Kratz, D.P., Feldman, D.R., Collins, W.D., Mlawer, E.J., Alvarado, M.J., Lawler, J.E., Anderson, L.W., Fahey, D.W. and Hunt, L.A. (2016) The spectroscopic foundation of radiative forcing of climate by carbon dioxide. *Geophysical Research Letters*, 43, 5318–5325. https://doi.org/10.1002/2016gl068837.

Pierrehumbert, R.T. (2010) *Principles of Planetary Climate*. Cambridge, UK: Cambridge, UK University Press.

Plass, G.N. (1956) The influence of the 15μ carbon-dioxide band on the atmospheric infra-red cooling rate. *Quarterly Journal of the Royal Meteorological Society*, 82, 310–324. https://doi.org/10.1002/qj.49708235307.

Shine, K.P., Fouquart, Y., Ramaswamy, V., Solomon, S. and Srinivasan, J. (1995) Radiative forcing: radiative forcing of climate change and an evaluation of the IPCC IS92 emission scenarios. In: Houghton, J.T., et al. (Eds.) *Intergovernmental Panel on Climate Change*. UK: Cambridge University Press.

Shine, K.P. and Myhre, G. (2020) The spectral nature of stratospheric temperature adjustment and its application to halocarbon radiative forcing. *Journal of Advances in Modeling Earth Systems*, 12, e2019MS001951. https://doi.org/10.1029/2019ms001951.

Zhong, W.Y. and Haigh, J.D. (2013) The greenhouse effect and carbon dioxide. *Weather*, 68, 100–105. https://doi.org/10.1002/wea.2072.

How to cite this article: Shine, K.P. & Perry, G.E. (2023) Radiative forcing due to carbon dioxide decomposed into its component vibrational bands. *Quarterly Journal of the Royal Meteorological Society*, 1–11. Available from: https://doi.org/10.1002/qj.4485

APPENDIX

Dufresne *et al.* (2020) present a highly informative analysis of the details of CO_2 RF and how it depends on the change in emission height and the total absorption of the atmosphere (and how these contributions vary with wavenumber). Here a simpler illustration is presented as to why, in some spectral regions, increasing infrared intensity increases RF, while in others it decreases RF.

RF is strongly related to the rate of change of atmospheric infrared absorptance A, as CO_2 concentrations are increased. For a homogeneous path of length l, the CO_2 absorptance can be written in terms of transmittance Tr such that

$$A = 1 - \mathrm{Tr} = 1 - \exp(-kCNl), \tag{A1}$$

where k is the absorption cross-section (in $\mathrm{cm}^2 \cdot \mathrm{molecule}^{-1}$), which varies strongly with wavenumber, N is the number concentration of air molecules and C is the mole fraction of CO_2.

The rate of change of A with CO_2 concentration is

$$\frac{dA}{dC} = kNl \exp(-kCNl). \tag{A2}$$

The variation of this with k is then given by

$$\frac{d}{dk}\left(\frac{dA}{dC}\right) = Nl(1 - kCNl)\ \exp(-kCNl), \tag{A3}$$

the sign of which depends on whether $(1 - kCNl)$ is positive or negative. For a given CNl, if k is sufficiently small then $\left(\frac{dA}{dC}\right)$, and hence the forcing, increases as k increases; at higher k, $\left(\frac{dA}{dC}\right)$ decreases as k increases.